

Electronic Supplementary Information

Secondary Interaction-Manipulated Metal–Organic Crystalline Nanotube Array for Gas Sensing

Jieying Hu,^{#a} Jian-Ze Xiao,^{#b} Wei-Ming Liao,^{*a} Shoujie Liu,^c Jianming Li,^a Yonghe He,^a Lin Yu,^a Qiaohong Li,^b Gang Xu^{*bde} and Jun He^{*a}

^a *School of Chemical Engineering and Light Industry, Guangdong University of Technology, Guangzhou, 510006, P. R. China.*

^b *State Key Laboratory of Structural Chemistry, Fujian Institute of Research on the Structure of Matter, Chinese Academy of Sciences, Fuzhou, 350002, P. R. China.*

^c *Chemistry and Chemical Engineering of Guangdong Laboratory, Shantou, 515063, P. R. China.*

^d *University of Chinese Academy of Sciences, Beijing, 100049, P. R. China.*

^e *Fujian Science & Technology Innovation Laboratory for Optoelectronic Information of China, Fuzhou, 350108, P. R. China.*

These authors contributed equally to this work.

* Corresponding author: junhe@gdut.edu.cn; gxu@fjirsm.ac.cn; wmliao@gdut.edu.cn.

General procedure.

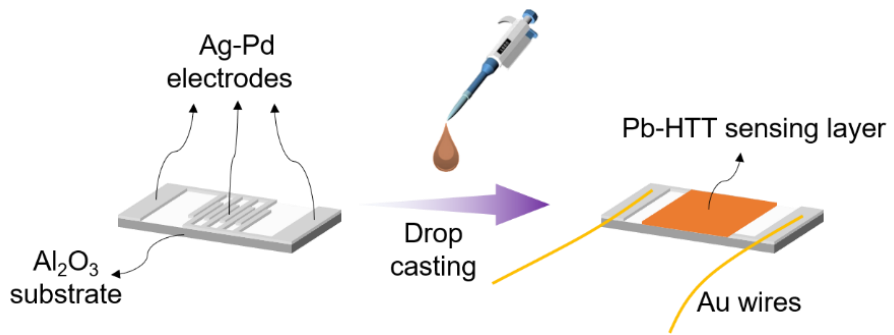
Starting materials, reagents, and solvents were purchased from commercial sources (*e.g.*, J&K, Aladdin, and Aldrich) and used without further purification. Solution ^1H NMR spectra were recorded on a 400 MHz Bruker superconducting magnet high-field NMR spectrometer at room temperature with tetramethylsilane (TMS) as internal standard. Chemical shifts (δ) are expressed in ppm relative to the residual solvent (*e.g.* chloroform ^1H : 7.26 ppm) reference. Coupling constants are expressed in hertz. FT-IR spectra were obtained using a Thermo-Fisher iS50R spectrophotometer. Thermogravimetric (TG) analyses were carried out using Netzsch STA449F5 thermal analyzer with a heating rate of 10 °C/min under N_2 and 5 °C/min under air atmosphere, respectively. Elemental analysis (EA) was obtained with a Vario Micro CUBE CHN elemental analyzer. Powder X-ray diffraction (PXRD) patterns were collected on a Rigaku Smart lab diffractometer with Cu K α radiation ($\lambda = 1.5418 \text{ \AA}$) at room temperature. The X-ray tube operated at a voltage of 40 kV and a current of 15 mA. Temperature-dependent PXRD patterns was collected using microcrystalline samples on a Rigaku Ultima IV diffractometer (40 kV, 40 mA, Cu K $\alpha 1$, $\lambda = 1.5418 \text{ \AA}$). The measurement parameters include a scan speed of 5 °C/min, a step size of 0.01 °, and a scan range of 2θ from 5 to 30°. The porosity and surface area analysis were performed using a Quantachrome Autosorb iQ gas sorption analyzer (version 5.21). The sample was outgassed at 6.58×10^{-5} torr with a 5 °C/min ramp to 105 °C and held at 105 °C for 8.2 hours. The sample was then held at vacuum until the analysis was run. The resistance data were measured on source meter equipment (Keithley 4200) with a single crystal solid, then electronic conductivity was determined by the function of $\sigma = L/(R \cdot S)$. X-ray photoelectron spectroscopic (XPS) measurements were conducted on a X-ray Photoelectron Spectroscopy System (Thermo Scientific K-Alpha). UV-Vis absorption Spectrum was collected in the UV-Visible Near Infra-red Spectrophotometer with Integrating Sphere (SHIMADZU, UV-3600 Plus). The morphology of the samples was investigated using scanning electron microscopy (SEM, TESCAN, CLARA, Czech). The high-resolution transmission electron microscope (HRTEM) images were collected on a transmission electron microscopy (JEOL JEM 2100F) with operating voltage at 200 kV. X-ray Absorption Fine Structure (XAFS) spectra were performed on the BL14W1 beamline of the Shanghai Synchrotron Radiation Facility (SSRF), and the data reduction and analysis of XANES and FT-EXAFS spectra were completed by using Athena software through the technical support provided by Ceshigo Research Service: www.cephigo.com.

Single crystal X-ray crystallography

Single crystal data for **Pb-HTT** were collected using a Rigaku Oxford SuperNova diffractometer using Ga K α radiation ($\lambda = 1.34138 \text{ \AA}$) at 80 K. Reflections were indexed and reduced by using SAINT V8.38A, and the files were corrected for absorption using SADABS-2016/2. The space group was assigned, the structure was solved by direct methods using ShelXS¹ and refined by full matrix least squares against F^2 with all reflections using ShelXL² of Olex2³ software packages. All non-hydrogen atoms were refined with anisotropic thermal parameters, and all hydrogen atoms were included in calculated positions and refined with isotropic thermal parameters riding on those of the parent atoms. As the ethylenediamine was disordered, RIGU and SIMU were used to restrain the atomic displacement parameters (ADP), DFIX was used to restrain the bond lengths and bond angles. In addition, several bad reflections with large error/esd values were also omitted. Crystallized ethylenediamine, DMF, CH₃OH and H₂O molecules in the pores were disordered and difficult to solve, therefore the related electron density peaks have been removed by the SQUEEZE subroutine in PLATON.⁴ The solvent mask was calculated and 1478 electrons were found in a volume of 5911 Å³ per unit cell. This is consistent with the presence of 3.5 C₂N₂H₈, 0.4 C₃H₇NO, 1 CH₃OH, 2 H₂O per asymmetric unit, indicating a formula of [Pb₅(HTT)₂(C₂N₂H₉)₂]·3.5C₂N₂H₈·0.4C₃H₇NO·CH₃OH·2H₂O for **Pb-HTT**. Details of refinement results are listed in Table S1.

DFT calculation

We have employed the Vienna Ab Initio Package (VASP)^{5,6} to perform all the density functional theory (DFT) calculations within the generalized gradient approximation (GGA) using the Perdew-Burke-Ernzerhof (PBE)⁷ formulation. We have chosen the projected augmented wave (PAW) potentials^{8,9} to describe the ionic cores and take valence electrons into account using a plane wave basis set with a kinetic energy cutoff of 400 eV. Partial occupancies of the Kohn–Sham orbitals were allowed using the Gaussian smearing method and a width of 0.05 eV. The electronic energy was considered self-consistent when the energy change was smaller than 10⁻⁵ eV. A geometry optimization was considered convergent when the force change was smaller than 0.02 eV/Å. Grimme's DFT-D3 methodology¹⁰ was used to describe the dispersion interactions. The adsorption energies E_{ads} were calculated by the following formula: E_{ads} = E_{gas on Pb-HTT} – E_{Pb-HTT} – E_{gas molecule}, where E_{gas on Pb-HTT}, E_{Pb-HTT} and E_{gas molecule} are the energy of gas molecule adsorbed on **Pb-HTT**, the energy of clean **Pb-HTT**, and the energy of isolated gas molecule in a cubic periodic box with a side length of 20 Å and a 1 × 1 × 1 Monkhorst-Pack *k*-point grid for Brillouin zone sampling, respectively.



Scheme S1. Fabrication of gas sensor devices.

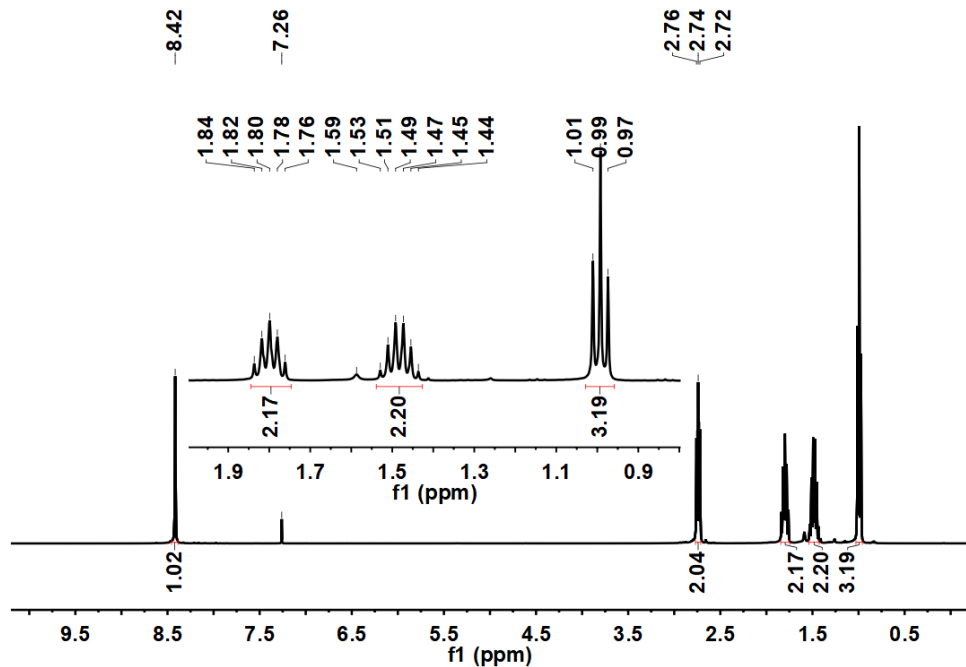


Fig. S1. Solution ^1H NMR spectrum of HVaTT (CDCl_3 , 400 MHz).

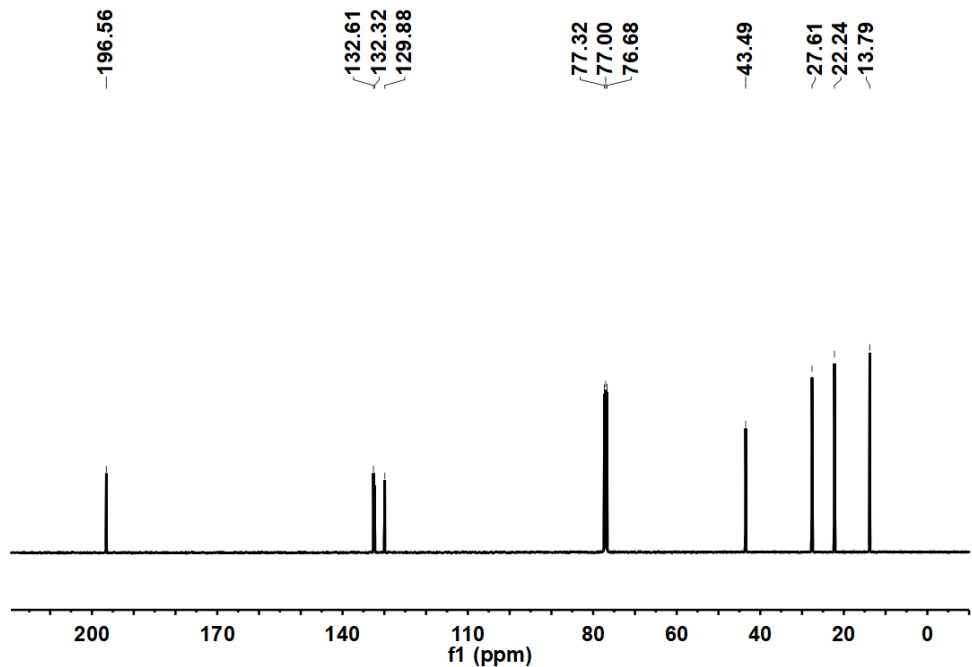


Fig. S2. Solution ^{13}C NMR spectrum of HVaTT (CDCl_3 , 101 MHz).

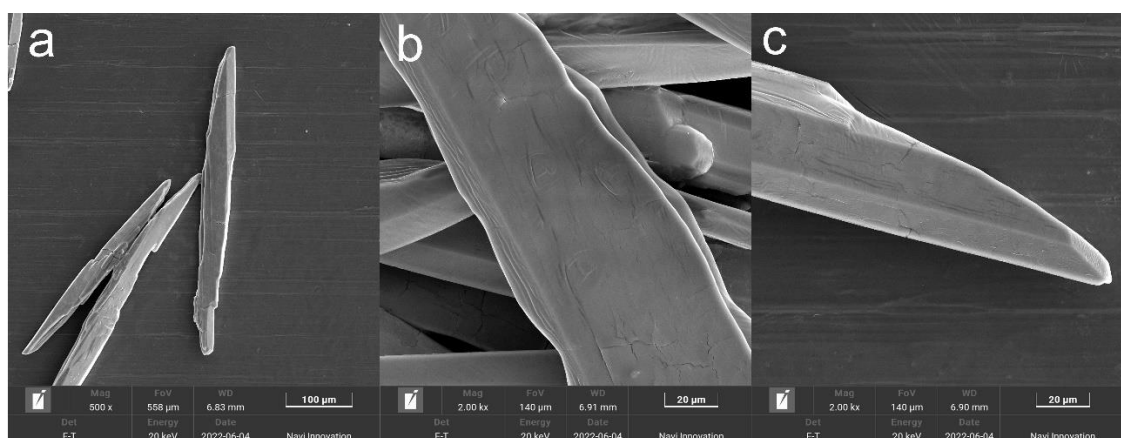


Fig. S3. SEM images of Pb-HTT crystals with the scale bar of (a) 100, and (b, c) 20 μm , respectively.

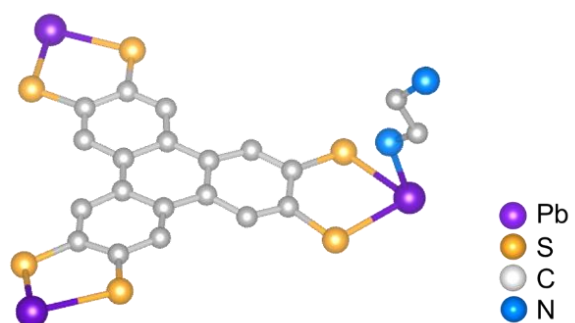


Fig. S4. The asymmetric unit of Pb-HTT. (Hydrogen atoms are omitted for clarity).

Search Overview

Search:	search1
Date/Time done:	Thu Sep 22 15:03:15 2022
Database(s):	CSD version 5.43 updates (Mar 2022) CSD version 5.43 (November 2021) CSD version 5.43 updates (Jun 2022)
Restriction Info:	No refcode restrictions applied
Filters:	None
Percentage Completed:	100%
Number of Hits:	84

Single query used. Search found structures that:

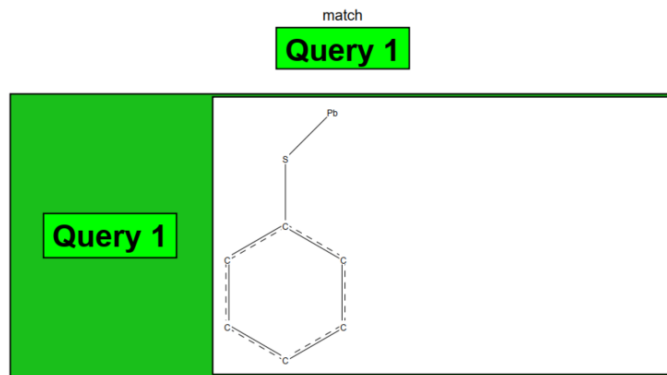


Fig. S5. Structure fragment and search conditions for the single crystals containing Pb-S bonds and/or secondary Pb···S interactions.

The above Pb···S-phenyl fragment in Figure S3 was taken as a query in CCDC database to search the coordination bond and secondary interaction between Pb and S, and the results of 70 hits were summarized in Table S3. It's found that all of the Pb-S bond lengths located below 3.20 Å, and most of the Pb···S secondary interaction distances located above 3.20 Å while several were between 2.95 and 3.20 Å. Based on the principles of rigor and adequacy, the Pb···S secondary interaction was tentatively attributed to the interaction with distance between 3.20 and 3.80 Å (Pb and S van der Waals radii).

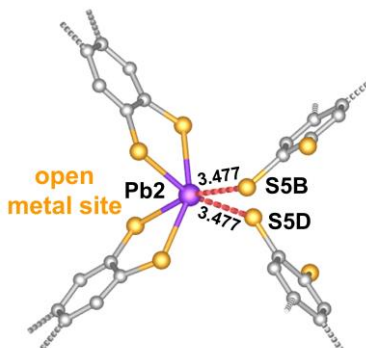


Fig. S6. The structure of Pb2 center. Coordination environment and secondary interactions of Pb2 center.

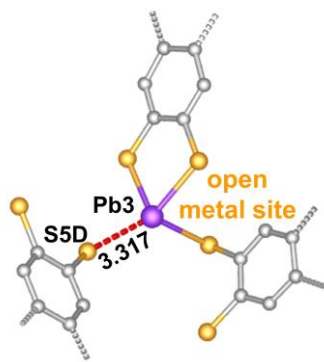


Fig. S7. The structure of Pb3 center. Coordination environment and secondary interactions of Pb3 center.

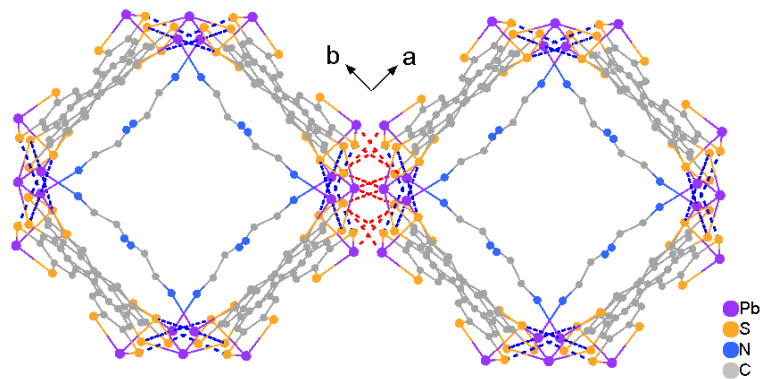


Fig. S8. The secondary $\text{Pb}\cdots\text{S}$ interactions in **Pb-HTT** array. Blue and red dots represent intra-tube and inter-tube secondary interactions, respectively.

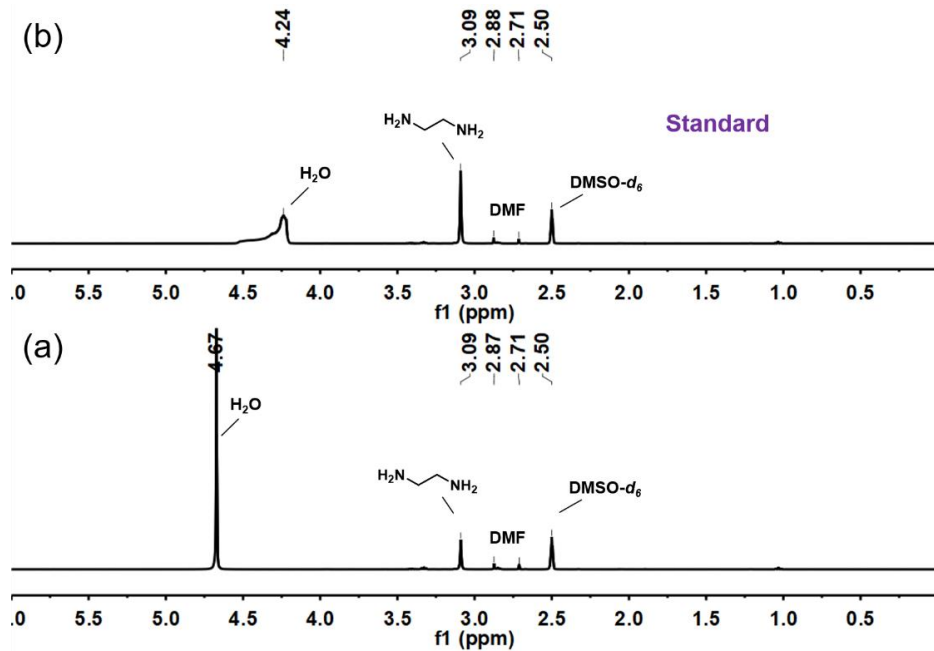


Fig. S9. Solution ^1H NMR spectra (DMSO- d_6 , 400 MHz) for verifying the presence of ethylenediamine. (a) **Pb-HTT** dissolved in DMSO- d_6 (0.6 mL) and deuterated hydrochloric

acid (20 μ L), (b) the spectrum of sample (a) being added the standard sample of ethylenediamine.

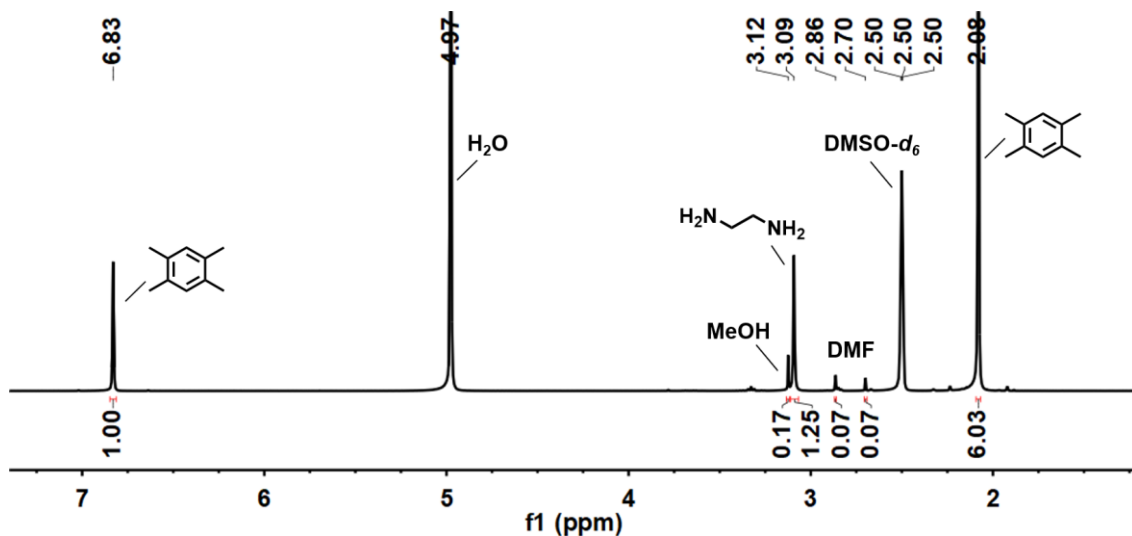


Fig. S10. Solution ^1H NMR spectra (DMSO- d_6 , 400 MHz) for verifying the amount of ethylenediamine. **Pb-HTT** (7.60 mg) and internal standard 1,2,4,5-tetramethylbenzene (3.70 mg) were dissolved in DMSO- d_6 (0.6 mL) and deuterated hydrochloric acid (20 μ L), indicating an amount of 13.62 wt%, 1.40 wt% and 1.24 wt% for ethylenediamine, methanol and DMF, respectively, which is quite close to the result of 13.74 wt%, 1.42 wt%, 1.25 wt% from the crystal data.

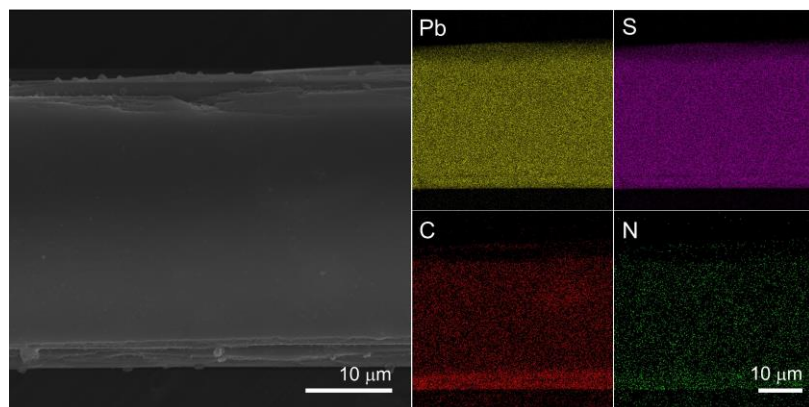


Fig. S11. Elemental mapping images of **Pb-HTT**.

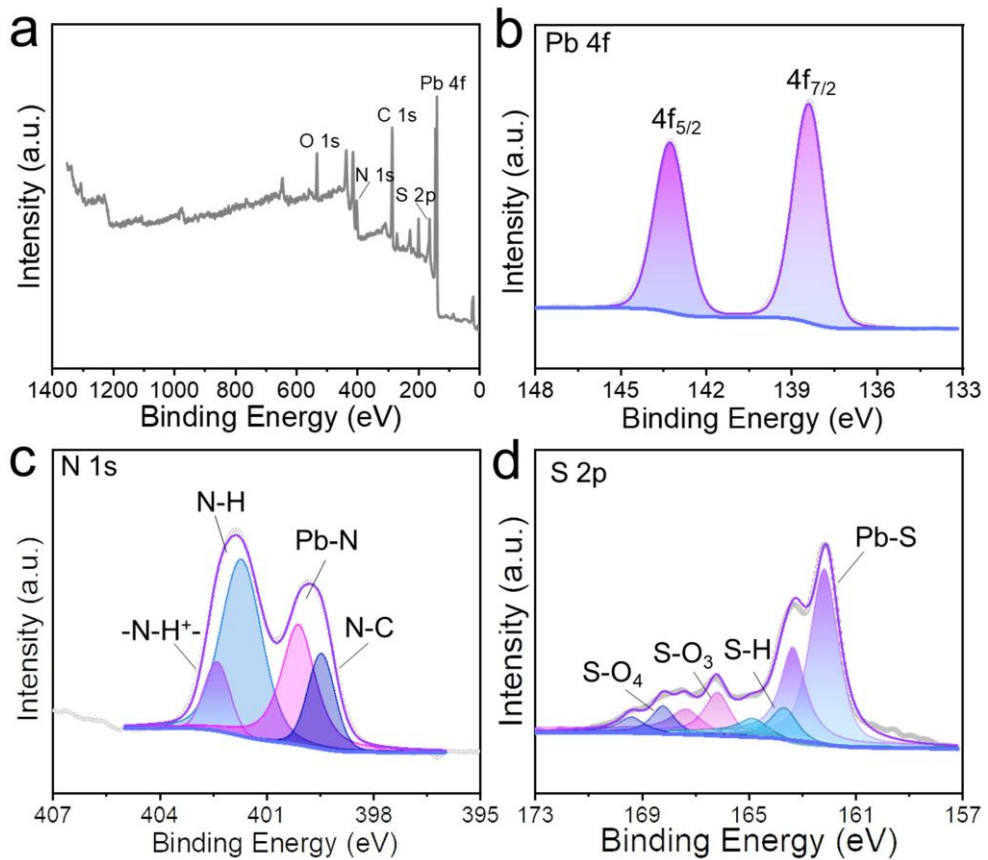


Fig. S12. XPS spectra of **Pb-HTT**. (a) Full region; (b) Pb 4f region; (c) N 1s region; d) S 2p region. Deconvolution of the S 2p signal generates four sets of doublets. The doublets at 162.16 and 163.34 eV are derived from the Pb–S coordination. The weak doublets at 163.64 and 164.82 eV can be ascribed to the partially uncoordinated –SH residues. The peaks (from 166.15 to 169.38 eV) indicate the existence of –S–O– bond resulted from concomitant ligand oxidation ¹¹⁻¹³.

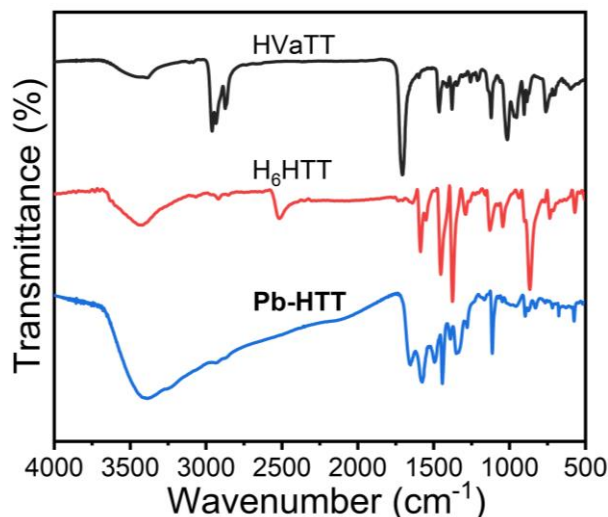


Fig. S13. FT-IR spectra of HVaTT, H₆HTT and **Pb-HTT**. It features a strong absorption at 1700 cm⁻¹ for the carbonyl stretching of the thioester functional group. The stretching peaks at

2800-3000 cm^{-1} are in accordance with aliphatic C-H groups. FT-IR spectrum of H₆HTT shows a S-H stretching peak at 2507 cm^{-1} which disappeared after coordination with Pb^{II}.

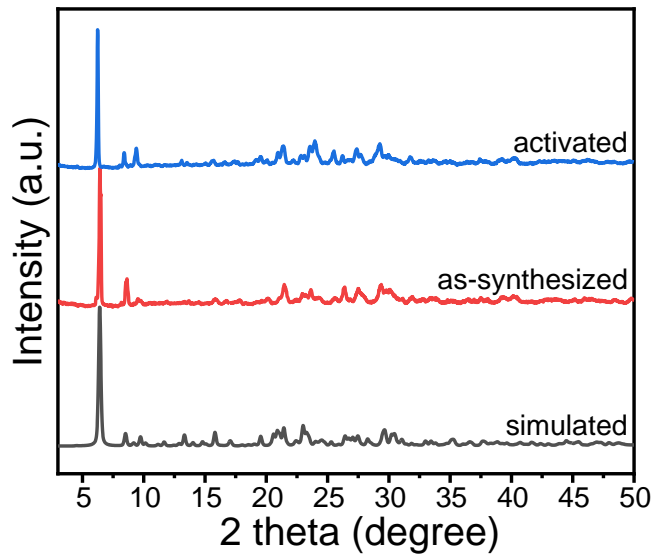


Fig. S14. PXRD patterns for **Pb-HTT**: (a) simulated, (b) as-synthesized and (c) after activation.

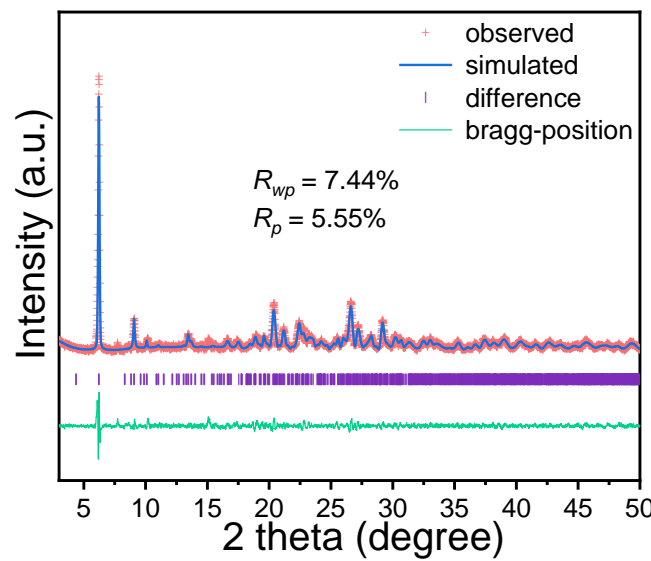


Fig. S15. Rietveld Refinement of the experimental PXRD pattern ($\lambda = 1.5418 \text{ \AA}$) of **Pb-HTT**. The R_{wp} and R_p are equal to 7.44% and 5.55%, respectively.

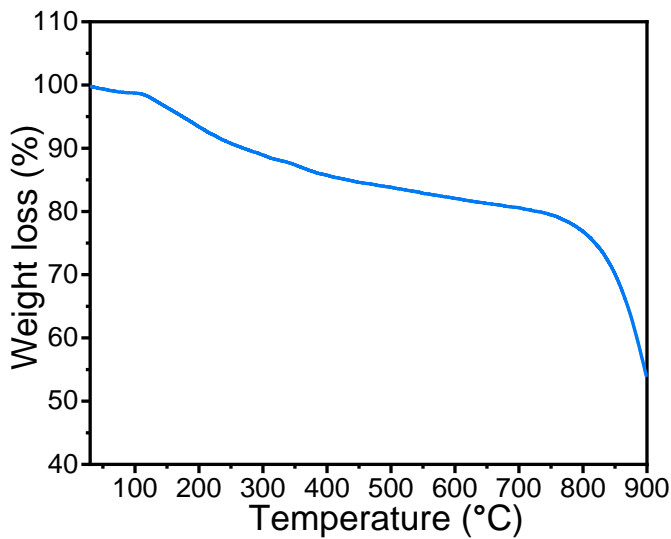


Fig. S16. TG curve of **Pb-HTT** recorded under N_2 atmosphere (heating rate: 5 °C/min).

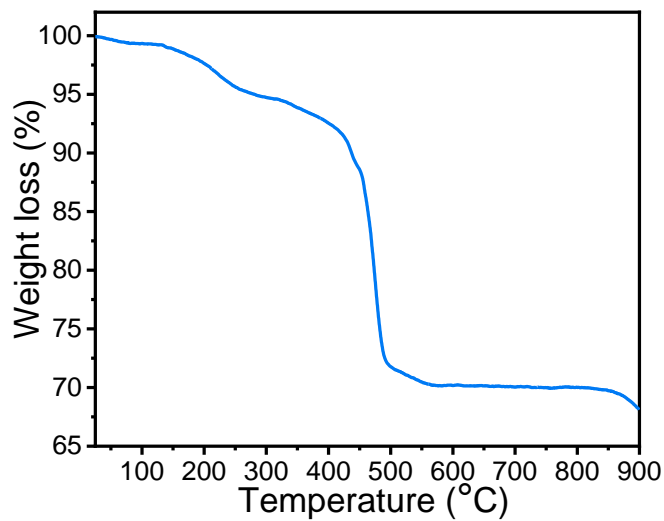


Fig. S17. TG curve of **Pb-HTT** recorded in air (heating rate: 5 °C/min).

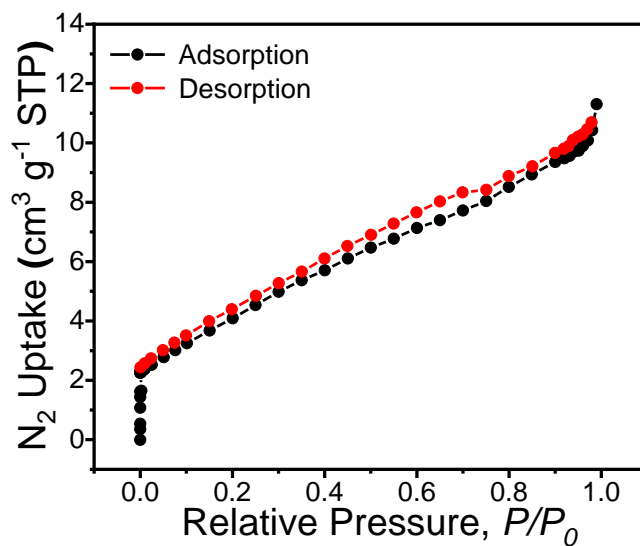


Fig. S18. N_2 adsorption-desorption isotherms of **Pb-HTT** at 77 K.

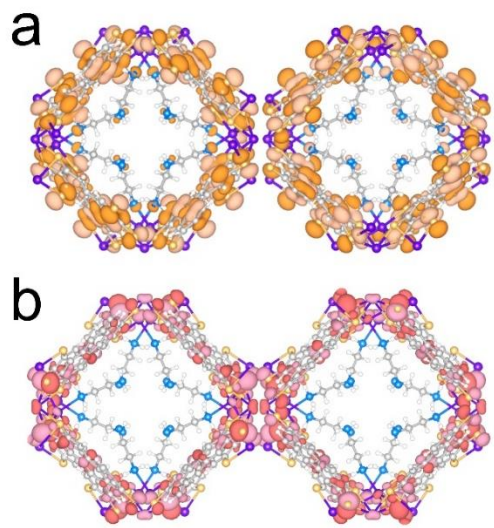


Fig. S19. Frontier electron density of (a) CBM and (b) VBM.

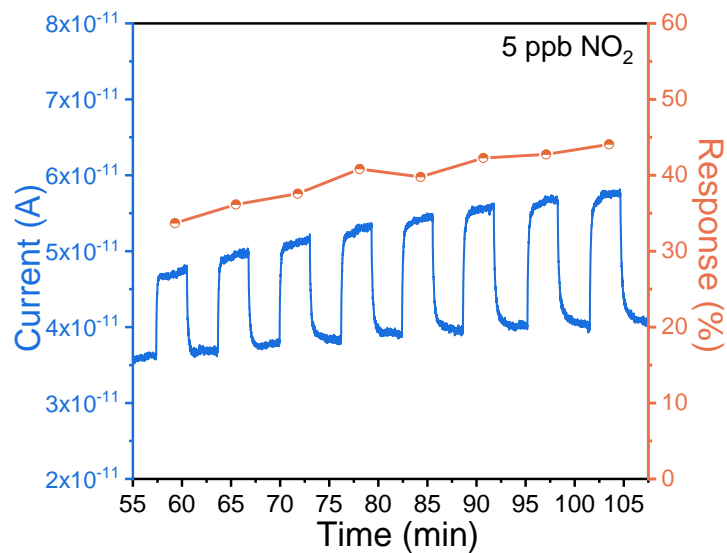


Fig. S20. NO_2 sensing of **Pb-HTT**. Current signal curves and response values towards 5 ppb NO_2 sensing.

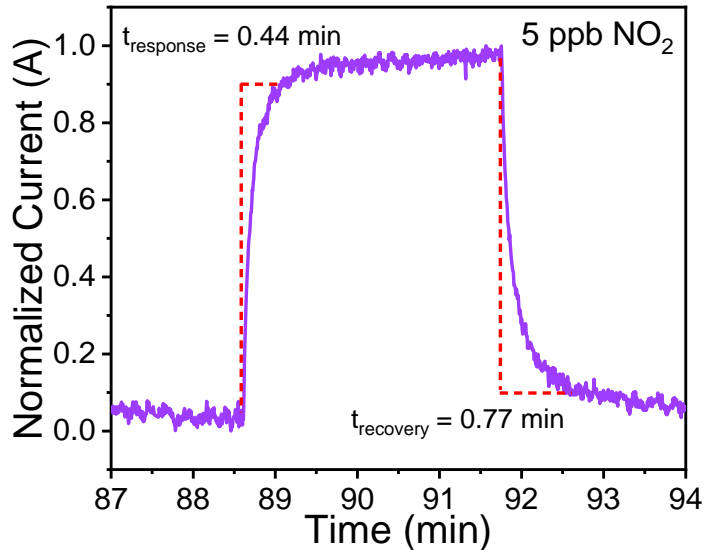


Fig. S21. Response and recovery time towards 10 ppm NO₂.

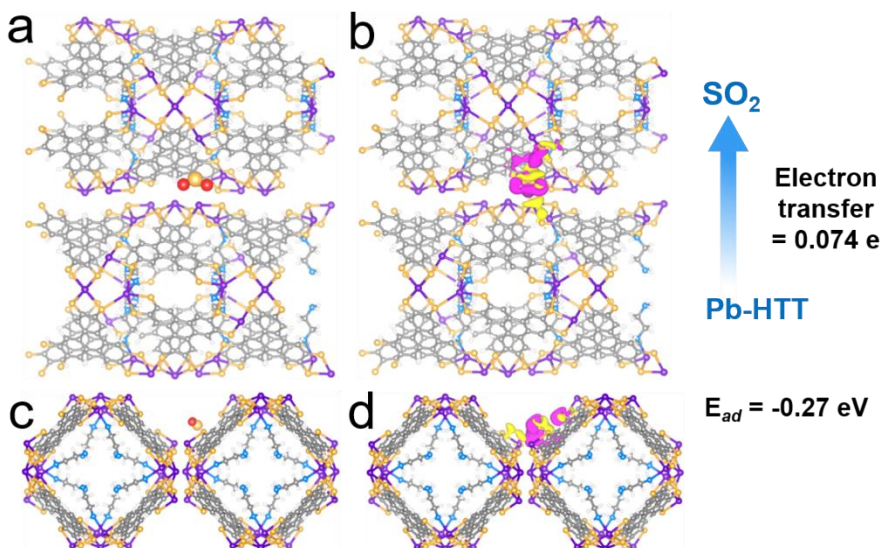


Fig. S22. DFT calculation of Pb-HTT towards SO₂. Adsorption configuration of SO₂ on Pb-HTT viewed along (a) *b*-axis and (c) *c*-axis; Electron density difference of the corresponding model viewed along (b) *b*-axis and (d) *c*-axis. Pink indicates electron accumulation and yellow indicates electron depletion. The isovalue is set to be $0.0003 \text{ e } \text{\AA}^{-3}$.

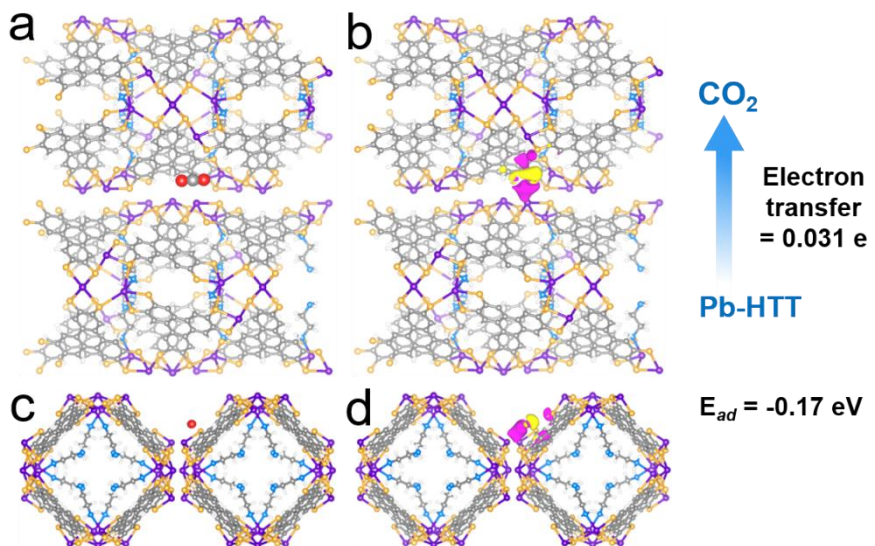


Fig. S23. DFT calculation of **Pb-HTT** towards CO_2 . Adsorption configuration of CO_2 on **Pb-HTT** viewed along (a) *b*-axis and (c) *c*-axis; Electron density difference of the corresponding model viewed along (b) *b*-axis and (d) *c*-axis. Pink indicates electron accumulation and yellow indicates electron depletion. The isovalue is set to be $0.0003 \text{ e } \text{\AA}^{-3}$.

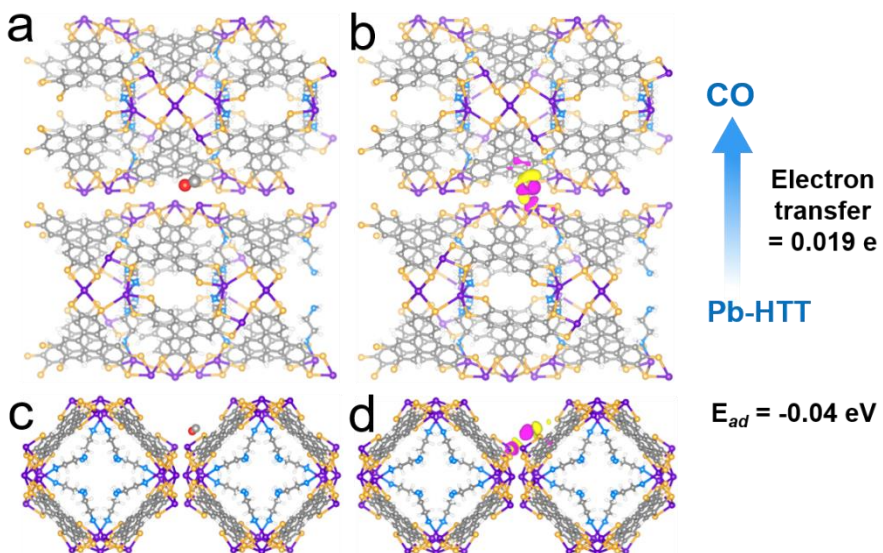


Fig. S24. DFT calculation of **Pb-HTT** towards CO. Adsorption configuration of CO on **Pb-HTT** viewed along (a) *b*-axis and (c) *c*-axis; Electron density difference of the corresponding model viewed along (b) *b*-axis and (d) *c*-axis. Pink indicates electron accumulation and yellow indicates electron depletion. The isovalue is set to be $0.0003 \text{ e } \text{\AA}^{-3}$.

Table S1. Crystallographic refinement parameters and results of **Pb-HTT**.

Compound	Pb-HTT
CCDC number	2129174
Empirical formula	$[\text{Pb}_5(\text{HTT})_2(\text{C}_2\text{N}_2\text{H}_9)_2] \cdot 3.5\text{C}_2\text{N}_2\text{H}_8 \cdot 0.4\text{C}_3\text{H}_7\text{N}$ $\text{O} \cdot \text{CH}_3\text{OH} \cdot 2\text{H}_2\text{O}$
Formula weight	2295.02
Temperature/K	80
Crystal system	tetragonal
Space group	<i>P</i> 4/ <i>ncc</i> (130)
<i>a</i> /Å	27.4995(14)
<i>b</i> /Å	27.4995(14)
<i>c</i> /Å	19.1795(12)
α°	90.00
β°	90.00
γ°	90.00
Volume/Å ³	14504.0(17)
Z	8
<i>D</i> _c /g·cm ⁻³	2.102
μ/mm^{-1}	17.223
<i>F</i> (000)	8584.0
<i>R</i> ₁ ^a (<i>I</i> > 2σ(<i>I</i>))	0.0586
<i>wR</i> ₂ ^b (all data)	0.1424
GOF on <i>F</i> ²	1.051

^a $R_1 = \sum(|F_o| - |F_c|) / \sum |F_o|$; ^b $wR_2 = (\sum w(F_o^2 - F_c^2)^2 / \sum w(F_o^2)^2)^{1/2}$

Table S2. Information of single-crystal structures containing the fragment of Pb···S-phenyl.

Compound Name	CCDC Code	CCDC Number	Bond/Å	Secondary Interaction/Å	Refs.
compound 3	ALIJAG	205059	2.709	3.296	14
C ₇₂ H ₁₀₂ Pb ₃ S ₆ (compound 8b)	CAWZIJ	1121012	2.553-2.896		15
[(C ₆ H ₅) ₄ As]-[Pb(SC ₆ H ₅) ₃] (1)	CUKRUU		2.619-2.647		16
Ph ₃ PbSPh	DALCEY		2.515		17
[NPr ⁿ ₄][Pb(SPh) ₃] (2)	DELFOPO	1138563	2.633-2.696		18
Pb-[SC ₆ H ₄ (CH ₂ NMe ₂)-2][N(SiMe ₃) ₂] (6)	DONTAD	1006880	2.647		19
[Pb(C ₆ F ₅ S)2(C ₅ H ₅ N) ₂] _n	EREWUU	828434	2.652	3.614/3.618	20
[(4-Me ₃ NC ₆ H ₄ S) ₆ Pb ₃][PF ₆] ₆ (7)	FAKBIE	825269	2.712-2.981		21
[(4-Me ₃ NC ₆ H ₄ S) ₃ Pb][BPh ₄] ₂ (8)	FAKBOK	825270	2.631-2.874	3.168/3.339	21
[(4-Me ₃ NC ₆ H ₄ S) ₂ Pb(py)] ₂ [BPh ₄] ₄ (9)	FAKBUQ	825271	2.607/2.669	3.106	21
[(4-Me ₃ NC ₆ H ₄ S) ₂ Pb(bipy) _{0.5}][BPh ₄] ₂ (10)	FAKCAX	825272	2.596/2.646	3.176	21
(13) Pb(SAr ^{Pr6}) ₂	FIFQES	955308	2.575/2.584		22
(14) Pb(SAr ^{Pr8}) ₂	FIFQIW	955309	2.580/2.594		22
[(L ^{M_e} Pb ₂] ²⁺	FIMLET	243457	2.554/2.640	3.465/3.824	23
[Pb{Ph ₂ P(O)C ₆ H ₄ S-2}] ₂]·1/2CH ₃ OH·2H ₂ O (3)	FIQVIM	961451	2.647		24
compound 7	GAGXES	243400	2.608		25
compound 8	GAGXIW	243401	2.595-2.602		25
compound 9	GAGXOC	243403	2.595/2.599	3.743	25
compound 10	GAGXUI	243402	2.696-3.000	2.993-3.422	25
[Pb ₁₀ {S-2,6-(CH ₃) ₂ C ₆ H ₃ } ₂₀] (1)	GANKOW	246835	2.558-3.175	3.555/3.627	26
[Pb ₆ S{S-2,6-(CH ₃) ₂ C ₆ H ₃ } ₁₀ -(C ₄ H ₈ O) ₄] (2)	GANKUC	246836	2.627-3.121	3.506/3.536	26
[Pb ₈ O ₂ {S-2,6-(CH ₃) ₂ C ₆ H ₃ } ₁₂] (3)	GANLAJ	246837	2.562-3.100	3.349-3.614	26
[Pb ₁₄ O ₆ {S-2,6-(CH ₃) ₂ C ₆ H ₃ } ₁₆] (4)	GANLEN	246838	2.627-3.055	3.228-3.701	26
compound 2	GUKYUH	713332	2.679		27
[Pb(SC ₆ H ₄ S)(dien)] _n	HAVDAL	879208	2.961/3.072	3.271/3.652	28
[Pb ₃ (SC ₆ H ₄ S) ₃ (en)] _n	HIXCUN	678533	2.745-2.908	3.037-3.513	29
[Pb ₂ (S ₂ C ₆ H ₂ S ₂)(en)] _n	HIXDAU	678534	2.580/2.619	2.948/3.03	29
[Pb ₃ (C ₆ S ₆)] _n	HIXDEY	678535	3.073		29
PbBDT	IBUDOC	2084844	2.761-2.931		30
Pb(SR _f) ₂ ·THF 2a	KOYFEJ		2.639		31
[PbL ⁴ (ClO ₄) ₂]	LEHNOB	1204986	3.141/3.175		32
[(2,6-Me ₂ C ₆ H ₃ S) ₂ Pb] ₂ (dppe) (11)	LEZKIM	827119	2.608/2.617		33
[(2,6-Me ₂ C ₆ H ₃ S) ₂ Pb] ₃ (dmpe) (10)	LEZKOS	827118	2.643-2.987		33
[(2,6-Me ₂ C ₆ H ₃ S) ₂ Pb] ₂ (tmeda) (9)	LEZKUY	827117	2.558-3.028		33
[Pb{2-(Ph ₂ PO)-6-(Me ₃ Si)C ₆ H ₃ S} ₂] 3	MAWNH		2.644/2.646		34
[Pb{2-(Ph ₂ P(O)CH ₂)C ₆ H ₄ S} ₂] 4	MAWNON	142548	2.584/2.617		34
[Pb{2-(Ph ₂ P(S)CH ₂)C ₆ H ₄ S} ₂] 5	MAWNUT	142549	2.550-3.151		34

[Pb{2,6-(Ph ₂ P(S)CH ₂) ₂ C ₆ H ₃ S} ₂] (6)	MAWPAB	142550	2.659-3.020	3.370/3.386	34
compound 10	MIMQOQ	929509	2.598/2.613		35
compound 9	MIMQUW	929508	2.634/2.628		35
[Et ₄ N][{(MeC ₆ H ₃ S ₂)PbPh ₂ Cl}] (3)	NETDAR	1218793	2.515/2.632		36
Tbt(TbtS)Pb (2)	NOMRIQ		2.498		37
[(Cp'(CO) ₂ Mn)Pb(SMes) ₃] ⁺ (A4)	POLREN	1236512	2.594-2.613		38
compound 6	QOHKAZ	1243525	2.574		39
[\{O(C ₆ H ₄ S) ₂ \}PbPh ₂] (1b)	QORWOK	704628	2.531/2.536		40
[\{S(C ₆ H ₄ S) ₂ \}PbPh ₂] (2b)	QORWUQ	704629	2.531/2.521	3.280/3.782	40
[\{S(C ₆ H ₃ S) ₂ O\}PbPh ₂] (3b)	QORXAX	704630	2.519/2.522		40
[\{(PPh ₃) ₃ \}Cu ₅ (μ-SPh) ₇ Pb] (1)	QUTYAH	936688	2.633-2.741		41
[Pb(μ-SPh) ₄ {Cu(PPh ₃) ₂ } ₂] (2)	QUTYEL	936689	2.685-2.951		41
[Pb ₂ (μ-SPh) ₆ {Ag(PPh ₃) ₂ } ₂] (3)	QUVFOE	1051585	2.606-2.722		41
Pb(SC ₆ H ₅) ₂ (1)	RAVZET		2.671-2.837	3.373/3.519	42
β-Pb(SPh) ₂	RAVZET01	670193	2.648-2.861	3.474/3.704	43
α-Pb(SPh) ₂	RAVZET02	684203	2.556-2.805	3.444/3.448	43
[Pb(Tab) ₃](ClO ₄) _n (1)	RIPROY	650340	2.683-2.763	3.424/3.503	44
[(μ-Cl)Pb ₂ (stol)(μ-stol) ₂] _n (1)	UTERUI	1451294	2.717-2.961	3.348/3.375	45
[PbAg ₂ (μ-stol) ₂ (μ ₄ -stol) ₂] _n (2)	UTESAP	1451295	2.722/3.106		45
HTT-Pb	VATNIQ	1506170	2.666/2.714	3.258-3.666	46
Pb(SAr ^{Pri4}) ₂ (2)	VEYJOA	911152	2.566		47
LiPb(SAr ^{Me6}) ₃ (4)	VEYKAN	911151	2.669-2.678		47
{Pb(Br)(μ-SAr ^{Me6}) } ₂ (3)	VEYKOB	911149	2.724-2.810		47
[Pb(SC ₆ F ₅) ₂] _n	WEJMEE	610788	2.704-3.036		48
[PbL ¹ (MeOH)(H ₂ O)][ClO ₄] ₂ 1a	WEWZON		3.146/3.192		49
Pb ₅ O(SR _F) ₈ ·2C ₇ H ₈ (3)	WOTFAM	155933	2.854-3.180	3.625/3.633	50
Pb ₂ I(S-C ₆ H ₅) ₃	WUDTOH	1945769	2.730-3.164		51
Pb ₂ Br(S-C ₆ H ₅) ₃	WUDWAW	1945770	2.732-3.116		51
Pb ₂ Cl(S-C ₆ H ₅) ₃	WUDWEA	1945771	2.723-3.098		51
[(2,6-Me ₂ C ₆ H ₃ S) ₂ Pb(pyCOH)] ₂ (3)	XIRBUW	643476	2.626/2.664	3.174	52
[(2,6-Me ₂ C ₆ H ₃ S) ₂ Pb(pyOMe)] ₂ (4)	XIRCAD	643477	2.618/2.648	3.267	52
(2,6-Me ₂ C ₆ H ₃ S) ₂ Pb(pyNMe ₂) (5)	XIRCEH	643478	2.607/2.621		52
{[Pb(Tab) ₂ (bpe)] ₂ (PF ₆) ₄ } _n ·3nMeCN	YOTJOI	1031160	2.630/2.673	3.379	53

Table S3. Previously reported sensing materials towards NO₂ without light irradiation and with a response time less than one minute.

Materials	Conc./ppm	Temp./°C	Response/%	LOD/ppb	T _{res} /T _{rec} /min	Refs.
Pb-HTT	10	RT	1005 ^b	0.0206 ^d	0.04/0.40	<i>This work</i>
Pb-HTT	0.005	RT	39.64 ^b	/	0.44/0.77	<i>This work</i>
ZIF-8 derived-ZnFe ₂ O ₄ -rGO	2	RT	112.3 ^b	0.149 ^c	0.27 / 4.07	54
PbBDT OIHSI nanosheets	0.4	RT	/	0.51 ^c	0.27/0.79	55
few-layered MoS ₂ nanosheets	0.5	RT	530 ^a	27 ^c	0.90/20.67	56
Cu ₂ O/rGO	1	RT	520 ^a	32 ^c	0.49/0.76	57
PbS nanowires	50	RT	1750 ^a	36 ^c	0.05/2.47	58
Pd-SnO ₂ /rGO	100	RT	792 ^b	37.8 ^c	0.95/0.37	59
MIL-101(Cr)⊂PEDOT(45)	0.2	RT	0.9 ^a	60 ^c	<0.5 / Non	60
PbS CQDs	50	RT	2170 ^a	84 ^c	0.2/0.62	61
ZIF-8/Au NW	20	RT	0.9 ^b	190 ^c	0.12 / 11.5	62
PbCdSe QD gels	1.32	RT	75 ^b	3 ^d	0.52/1.05	63
ZnCo-ZIF/GN-120	100	RT	5461 ^a	10 ^d	0.02 / 0.2	64
γ-Bi ₂ MoO ₆ /GNCs	10	RT (25% RH)	5086 ^a	10 ^d	0.06 / 0.93	65
MoS ₂ /ZnO	5	RT	3050 ^b	50 ^d	0.67 / 16.67	66
SnO ₂ /rGO	1	RT	380 ^a	50 ^d	0.23/3.16	67
CuO/rGO	5	RT	400.8 ^b	50 ^d	0.11/0.91	68
N-doped MoS ₂	10	RT	28 ^b	125 ^d	0.37/1.82	69
PbS@MoS ₂	1	RT	320 ^a	200 ^d	<0.17/non	70
borophene	100	RT	422 ^b	200 ^d	0.50/3.33	71
WO ₃ /S/rGO	20	RT	14950 ^b	250 ^d	01/0.93	72
NiO/CuO	100	RT	7716 ^b	1000 ^d	0.03/-	73
CuO	4	RT	2810 ^a	1000 ^d	0.36/0.7	74

^aR = R_a/R_g or R_g/R_a, ^bR=(R_g-R_a)/R_a = ΔR/R_a, ^ctheoretical LOD, ^dexperimental LOD.

References

1. G. M. Sheldrick, *Acta Crystallogr. A*, 2008, **64**, 112-122.
2. G. M. Sheldrick, *Acta Crystallogr. C Struct. Chem.*, 2015, **71**, 3-8.
3. O. V. Dolomanov, L. J. Bourhis, R. J. Gildea, J. A. K. Howard and H. Puschmann, *J. Appl. Crystallogr.*, 2009, **42**, 339-341.
4. A. L. Spek, *Acta Crystallogr., Sect D Biol. Crystallogr.*, 2009, **65**, 148-155.
5. G. Kresse and J. Furthmüller, *Comput. Mater. Sci.*, 1996, **6**, 15-50.
6. G. Kresse and J. Furthmüller, *Phys. Rev. B Condens. Matter.*, 1996, **54**, 11169-11186.
7. J. P. Perdew, K. Burke and M. Ernzerhof, *Phys. Rev. Lett.*, 1996, **77**, 3865-3868.
8. P. E. Blochl, *Phys. Rev. B Condens. Matter.*, 1994, **50**, 17953-17979.
9. G. Kresse and D. Joubert, *Phys. Rev. B*, 1999, **59**, 1758-1775.
10. S. Grimme, J. Antony, S. Ehrlich and H. Krieg, *J. Chem. Phys.*, 2010, **132**, 154104.
11. A. J. Clough, N. M. Orchania, J. M. Skelton, A. J. Neer, S. A. Howard, C. A. Downes, L. F. J. Piper, A. Walsh, B. C. Melot and S. C. Marinescu, *J. Am. Chem. Soc.*, 2019, **141**, 16323-16330.
12. Z. Chen, Y. Cui, Y. Jin, L. Liu, J. Yan, Y. Sun, Y. Zou, Y. Sun, W. Xu and D. Zhu, *J. Mater. Chem. C*, 2020, **8**, 8199-8205.
13. R. Dong, M. Pfeffermann, H. Liang, Z. Zheng, X. Zhu, J. Zhang and X. Feng, *Angew. Chem., Int. Ed.*, 2015, **54**, 12058-12063.
14. K. Jurkschat, K. Peveling and M. Schürmann, *Eur. J. Inorg. Chem.*, 2003, **2003**, 3563-3571.
15. P. B. Hitchcock, M. F. Lappert, B. J. Samways and E. L. Weinberg, *J. Chem. Soc. Chem. Comm.*, 1983, 1492-1494.
16. P. A. W. Dean, J. J. Vittal and N. C. Payne, *Inorg. Chem.*, 1984, **23**, 4232-4236.
17. M. G. Begley, C. Gaffney, P. G. Harrison and A. Steel, *J. Organomet. Chem.*, 1985, **289**, 281-293.
18. G. Christou, K. Folting and J. C. Huffman, *Polyhedron*, 1984, **3**, 1247-1253.
19. A. Pop, L. Wang, V. Dorcet, T. Roisnel, J.-F. o. Carpentier, A. Silvestru and Y. Sarazin, *Dalton Trans.*, 2014, **43**, 16459-16474.
20. S. E. Appleton, G. G. Briand, A. Decken and A. S. Smith, *Acta Crystallogr. Sect. E*, 2011, **67**, m714.
21. G. G. Briand, A. Decken, M. C. Finniss, A. D. Gordon, N. E. Hughes and L. M. Scott, *Polyhedron*, 2012, **33**, 171-178.
22. B. D. Rekken, T. M. Brown, J. C. Fettinger, F. Lips, H. M. Tuononen, R. H. Herber and P. P. Power, *J. Am. Chem. Soc.*, 2013, **135**, 10134-10148.
23. V. Lozan and B. Kersting, *Eur. J. Inorg. Chem.*, 2005, **2005**, 504-512.
24. P. Fernández, J. Romero, J. A. García-Vázquez, A. Sousa-Pedrares, L. Valencia, J. Zubieto and P. Pérez-Lourido, *J. Organomet. Chem.*, 2014, **750**, 1-6.
25. S. E. Appleton, G. G. Briand, A. Decken and A. S. Smith, *Dalton Trans.*, 2004, 3515-3520.
26. A. Eichhöfer, *Eur. J. Inorg. Chem.*, 2005, **2005**, 1683-1688.
27. J. He, C. Yang, Z. Xu, M. Zeller, A. D. Hunter and J. Lin, *J. Solid State Chem.*, 2009, **182**, 1821-1826.
28. D. L. Turner, K. H. Stone, P. W. Stephens, A. Walsh, M. P. Singh and T. P. Vaid, *Inorg. Chem.*, 2012, **51**, 370-376.
29. D. L. Turner, T. P. Vaid, P. W. Stephens, K. H. Stone, A. G. Dipasquale and A. L. Rheingold, *J. Am. Chem. Soc.*, 2008, **130**, 14-15.

30. Y. Wen, G.-E. Wang, X. Jiang, X. Ye, W. Li and G. Xu, *Angew. Chem., Int. Ed.*, 2021, **60**, 19710-19714.
31. D. Labahn, S. Brooker, G. M. Sheldrick and H. W. Roesky, *Z. Anorg. Allg. Chem.*, 1992, **610**, 163-168.
32. K. R. Adam, D. S. Baldwin, A. Bashall, L. F. Lindoy, M. McPartlin and H. R. Powell, *J. Chem. Soc. Dalton Trans.*, 1994, **2**, 237-238.
33. A. J. Rossini, A. W. Macgregor, A. S. Smith, G. Schatte, R. W. Schurko and G. G. Briand, *Dalton Trans.*, 2013, **42**, 9533-9546.
34. P. Pérez-Lourido, J. Romero, J. A. García-Vázquez, A. Sousa, Y. Zheng, J. R. Dilworth and J. Zubieto, *J. Chem. Soc. Dalton Trans.*, 2000, DOI: 10.1039/A908496G, 769-774.
35. B. M. Barry, B. W. Stein, C. A. Larsen, M. N. Wirtz, W. E. Geiger, R. Waterman and R. A. Kemp, *Inorg. Chem.*, 2013, **52**, 9875-9884.
36. V. Chandrasekhar, A. Chandrasekaran, R. O. Day, J. M. Holmes and R. R. Holmes, *Phosphorus, Sulfur, and Silicon*, 1996, **115**, 125-139.
37. N. Kano, N. Tokitoh and R. Okazaki, *Organometallics*, 1997, **16**, 4237-4239.
38. F. Ettel, M. Schollenberger, B. Schiemenz, W. Imhof, G. Huttner and L. Zsolnai, *J. Organomet. Chem.*, 1994, **476**, 207-214.
39. J. H. Aupers, P. J. Cox, S. M. S. V. Doidge-Harrison, R. Alan howie, J. N. Low and J. L. Wardell, *Main Group Chem.*, 1999, **3**, 23-42.
40. S. González -Montiel, B. Flores-Chávez, J. G. Alvarado-Rodríguez, N. Andrade-López and J. A. Cogordan, *Polyhedron*, 2009, **28**, 467-472.
41. G. Gupta and S. Bhattacharya, *RSC Adv.*, 2015, **5**, 94486-94494.
42. A. D. Rae, D. C. Craig, I. G. Dance, M. L. Scudder, P. A. W. Dean, M. A. Kmestic, N. C. Payne and J. J. Vittal, *Acta Crystallogr. Sect. B*, 1997, **53**, 457-465.
43. M. Giffard, N. Mercier, B. t. Gravouille, E. Ripaud, J. m. Luc and B. Sahraoui, *CrystEngComm*, 2008, **10**, 968-971.
44. Z.-G. Ren, X.-Y. Tang, L. Li, G.-F. Liu, H.-X. Li, Y. Chen, Y. Zhang and J.-P. Lang, *Inorg. Chem. Commun.*, 2007, **10**, 1253-1256.
45. Z.-M. Wang, S.-M. Shen, X.-Y. Shen, F. Hu, A.-Q. Jia and Q.-F. Zhang, *J. Coord. Chem.*, 2016, **69**, 2263-2271.
46. J. Huang, Y. He, M.-S. Yao, J. He, G. Xu, M. Zeller and Z. Xu, *J. Mater. Chem. A*, 2017, **5**, 16139-16143.
47. B. D. Rekken, T. M. Brown, M. M. Olmstead, J. C. Fettinger and P. P. Power, *Inorg. Chem.*, 2013, **52**, 3054-3062.
48. H. Fleischer, C. Heller and D. Schollmeyer, *Acta Crystallogr. Sect. E*, 2006, **62**, m1365-m1367.
49. A. Bashall, M. McPartlin, B. P. Murphy, H. R. Powell and S. Waikar, *J. Chem. Soc. Dalton Trans.*, 1994, 1383-1390.
50. F. T. Edelmann, J.-K. F. Buijink, S. A. Brooker, R. Herbst-Irmer, U. Kilimann and F. M. Bohnen, *Inorg. Chem.*, 2000, **39**, 6134-6135.
51. A. H. Coffey, P. Yoo, D. H. Kim, Akriti, M. Zeller, S. Avetian, L. Huang, P. Liao and L. Dou, *Chem. – Eur. J.*, 2020, **26**, 6599-6607.
52. G. G. Briand, A. D. Smith, G. Schatte, A. J. Rossini and R. W. Schurko, *Inorg. Chem.*, 2007, **46**, 8625-8637.
53. F. Wang, F.-L. Li, M.-M. Xu, H. Yu, J.-G. Zhang, H.-T. Xia and J.-P. Lang, *J. Mater. Chem. A*, 2015, **3**, 5908-5916.
54. A. Bag, M. Kumar, D.-B. Moon, A. Hanif, M. J. Sultan, D. H. Yoon and N.-E. Lee, *Sens. Actuators, B* 2021, **346**, 130463.
55. Y. Wen, G. E. Wang, X. Jiang, X. Ye, W. Li and G. Xu, *Angew. Chem., Int. Ed.*, 2021, **60**, 19710-19714.

56. H. H. Hau, T. T. H. Duong, N. K. Man, T. Thi Viet Nga, C. Thi Xuan, D. Thi Thanh Le, N. Van Toan, C. M. Hung, N. Van Duy, N. Van Hieu and N. D. Hoa, *Sens. Actuators, A* 2021, **332**, 113137.
57. J. Pan, W. Liu, L. Quan, N. Han, S. Bai, R. Luo, Y. Feng, D. Li and A. Chen, *Ind. Eng. Chem. Res.*, 2018, **57**, 10086-10094.
58. H. Kan, M. Li, J. Luo, B. Zhang, J. Liu, Z. Hu, G. Zhang, S. Jiang and H. Liu, *IEEE Sensors J.* , 2019, **19**, 846-851.
59. H. Bai, H. Guo, C. Feng, J. Wang, B. Liu, Z. Xie, F. Guo, D. Chen, R. Zhang and Y. Zheng, *Appl. Surf. Sci.* , 2022, **575**, 151698.
60. B. Le Ouay, M. Boudot, T. Kitao, T. Yanagida, S. Kitagawa and T. Uemura, *J. Am. Chem. Soc.*, 2016, **138**, 10088-10091.
61. H. Liu, M. Li, O. Voznyy, L. Hu, Q. Fu, D. Zhou, Z. Xia, E. H. Sargent and J. Tang, *Adv. Mater.*, 2014, **26**, 2718-2724.
62. P. Li, H. Zhan, S. Tian, J. Wang, X. Wang, Z. Zhu, J. Dai, Y. Dai, Z. Wang, C. Zhang, X. Huang and W. Huang, *ACS Appl. Mater. Interfaces*, 2019, **11**, 13624-13631.
63. X. Geng, S. Li, L. Mawella-Vithanage, T. Ma, M. Kilani, B. Wang, L. Ma, C. C. Hewa-Rahinduwage, A. Shafikova, E. Nikolla, G. Mao, S. L. Brock, L. Zhang and L. Luo, *Nat. Commun.*, 2021, **12**, 4895.
64. L. He, W. Zhang, H. Wu and Y. Zhao, *ACS Appl. Nano Mater.*, 2021, **4**, 3998-4006.
65. L. He, H. Lv, L. Ma, W. Li, J. Si, M. Ikram, M. Ullah, H. Wu, R. Wang and K. Shi, *Carbon*, 2020, **157**, 22-32.
66. Y. Han, D. Huang, Y. Ma, G. He, J. Hu, J. Zhang, N. Hu, Y. Su, Z. Zhou, Y. Zhang and Z. Yang, *ACS Appl. Mater. Interfaces*, 2018, **10**, 22640-22649.
67. Z. Wang, T. Zhang, T. Han, T. Fei, S. Liu and G. Lu, *Sens. Actuators, B* 2018, **266**, 812-822.
68. H. Bai, H. Guo, J. Wang, Y. Dong, B. Liu, Z. Xie, F. Guo, D. Chen, R. Zhang and Y. Zheng, *Sens. Actuators, B* 2021, **337**, 129783.
69. R. Wu, J. Hao, S. Zheng, Q. Sun, T. Wang, D. Zhang, H. Zhang, Y. Wang and X. Zhou, *Appl. Surf. Sci.* , 2022, **571**, 151162.
70. J. Tan, J. Hu, J. Ren, J. Peng, C. Liu, Y. Song and Y. Zhang, *Chin. Chem. Lett.* , 2020, **31**, 2103-2108.
71. C. Hou, G. Tai, Y. Liu and X. Liu, *Nano Res.*, 2022, **15**, 2537-2544.
72. T. Wang, J. Hao, S. Zheng, Q. Sun, D. Zhang and Y. Wang, *Nano Res.*, 2018, **11**, 791-803.
73. H. Xu, J. Zhang, A. U. Rehman, L. Gong, K. Kan, L. Li and K. Shi, *Appl. Surf. Sci.* , 2017, **412**, 230-237.
74. S. Li, M. Wang, C. Li, J. Liu, M. Xu, J. Liu and J. Zhang, *Sci. China Mater.*, 2018, **61**, 1085-1094.